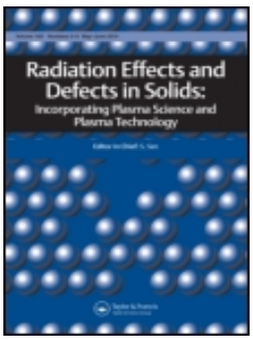

Taylor & Francis
Taylor & Francis Group

Radiation Effects and Defects in Solids
Incorporating Plasma Science and Plasma Technology

ISSN: 1042-0150 (Print) 1029-4953 (Online) Journal homepage: http://www.tandfonline.com/loi/grad20

Thermoluminescence studies of γ-irradiated nanocrystalline $Y_3Al_5O_{12}$

N.J. Shivaramu, B.N. Lakshminarasappa, K.R. Nagabhushana, Ramani & Fouran Singh

To cite this article: N.J. Shivaramu, B.N. Lakshminarasappa, K.R. Nagabhushana, Ramani & Fouran Singh (2014) Thermoluminescence studies of γ-irradiated nanocrystalline $Y_3Al_5O_{12}$, Radiation Effects and Defects in Solids, 169:8, 696-705, DOI: 10.1080/10420150.2014.922561

To link to this article: http://dx.doi.org/10.1080/10420150.2014.922561

Radiation Effects & Defects in Solids, 2014
Vol. 169, No. 8, 696–705, http://dx.doi.org/10.1080/10420150.2014.922561

Taylor & Francis
Taylor & Francis Group

Thermoluminescence studies of γ-irradiated nanocrystalline $Y_3Al_5O_{12}$

N.J. Shivaramu[a], B.N. Lakshminarasappa[a]*, K.R. Nagabhushana[b], Ramani[a] and Fouran Singh[c]

[a]*Department of Physics, Jnanabharathi Campus, Bangalore University, Bangalore 560 056, India;* [b]*Department of Physics (S & H), PES Institute of Technology, 100 Feet Ring Road, Banashankari 3rd Stage, Bangalore 560085, India;* [c]*Inter University Accelerator Centre, P.O. Box No. 10502, New Delhi 110 067, India*

(*Received 23 September 2013; final version received 5 May 2014*)

Nanocrystalline yttrium aluminum garnet ($Y_3Al_5O_{12}$) is synthesized by combustion technique. The X-ray diffraction (XRD) pattern of 900 °C annealed sample revealed a cubic structure. The average crystallite size is found to be 20.5 nm. γ-irradiated $Y_3Al_5O_{12}$ exhibits two thermoluminescence (TL) glows: a prominent one with a peak at ~410 K and another one with a peak at ~575 K. It is found that the TL glow peak intensity at 410 K increases, while its glow peak temperature is almost steady with an increase in the γ-dose. The effect of the heating rate on the TL glow curve is studied. It is found that T_{m1} shifts towards higher temperature region while the I_{m1} decreases with an increase in the heating rate. The TL glow curves are analyzed by Chen's peak shape method and the TL parameters are estimated.

Keywords: combustion synthesis; XRD; γ-irradiation; thermoluminescence; SEM

PACS: 81.20.Ka; 61.05.cp; 87.53.Bn; 78.60.Kn; 68.37.Hk

1. Introduction

Nanomaterials are very attractive phosphors for the cathode ray tube, flat panel displays, optical windows and solid-state lighting. Yttrium aluminum garnet (YAG) is commonly used as a host material in various solid-state lasers and fluorescent displays. YAG is proved to be an excellent optical component in laser and beam delivery systems. It is also known that YAG is one of the most creep resistant oxides and therefore is used as a host at high-temperature areas (*1*, *2*). The YAG has been investigated by material scientists due to its high optical transmission range (0.21–5.3 μm), excellent thermal conductivity (14.0 $W\,m^{-1}K^{-1}$), high refractive index (1.833), good dielectric constant (11) and elastic properties (*3–6*). YAG has a high melting point (1940 °C) too, with a specific gravity of 4.5 and a density of 4.5 $g\,cm^{-3}$, hardness 8.5 Mohs and has the ability to handle high fluences without any damage or significant wavefront distortion. YAG nanocrystals are also considered as very efficient scintillators for γ- and X-rays (*7*). YAG may be synthesized by a variety of routes such as solid-state reaction, sol–gel method (*7*), Stockbarger method (*8*), precipitation techniques (*9*) and solution combustion methods (*10*). Among these techniques, solution combustion method has several advantages since it is simple, fast, requires less energy and produces homogeneous and high purity crystalline oxides with a high surface area.

*Corresponding author. Email: bnlnarassappa@rediffmail.com

Thermoluminescence (TL) is a powerful technique to study charge carriers (electrons or holes). It is used to identify the nature of defects and their thermal stability in crystalline solids. TL is highly structure-sensitive, simple, a reliable technique and has wide applications in personal monitoring, archeological age determination of pottery, geological dating, etc. The principle of TL process is discussed in detail elsewhere (*11*, *12*). Recent studies indicate that luminescent nanomaterials have potential application in dosimetry caused by ionizing radiations (*13*, *14*). It may be noted that nanophosphors are shown as high-dose detectors in ionizing radiation. The influence of a high concentration of surface trapping centers and quantum confinement effect on the nanophosphor luminescence characteristics are important for radiation detection. TL behavior of YAG nanophosphors caused due to high γ-dose is reported in the present work with a detailed calculation of trapping parameters.

2. Materials and methods

The nanocrystalline YAG powder is prepared by solution combustion technique using yttrium oxide (Indian Rare Earth Ltd.), aluminum nitrate (Qualigens), nitric acid (Merck chemicals) and urea (Merck chemicals) as ingredients. Yttrium oxide is dissolved in dilute HNO_3 to obtain yttrium nitrate. Stochiometric amounts of yttrium nitrate, aluminum nitrate and urea are dissolved in a minimum quantity of double distilled water in a cylindrical Pyrex dish to obtain homogenous solution. The dish containing the homogeneous mixture is introduced into a muffle furnace maintained at $500 \pm 5\,^{\circ}C$. Initially, the solution begins to boil and forms foam and turns to flame less. Then, it undergoes dehydration followed by evaporation of a large amount of gasses and finally, it decomposes into powder form. The balanced reaction is given by:

$$3Y(NO_3)_3 + 5Al(NO_3)_3 + 20CH_4N_2O \rightarrow Y_3Al_5O_{12} + 20CO_2 \uparrow + 40H_2O \uparrow + 32N_2 \uparrow$$

The final product is found to be voluminous and nanocrystalline. Finally, the solid residue is transferred to a crucible and annealed at 900 °C in a muffle furnace for 6 h to remove the leftover carbon impurities, if any (*10*).

The synthesized powder is characterized by powder X-ray diffraction (PXRD) using 1.5406 Å Cu K_α radiations (The advanced D-8 X-ray diffractometer, Bruker AXS, Germany). Surface morphology of annealed YAG sample is obtained using a scanning electron microscope (SEM; JEOL-6490LV). A set of samples each of 10 mg are annealed and exposed to γ-rays for various doses in the range 1.0–14.0 kGy at room temperature. TL glow curves are recorded using a Harshaw thermoluminescence dosimeter reader (model 3500) fitted with a 931B PMT.

3. Results and discussion

Figure 1(a) shows the XRD pattern of 900 °C annealed combustion synthesized YAG. The XRD pattern is compared with standard Joint Committee on Powder Diffraction Standards (JCPDS) file (Card No.35–0810). The XRD pattern is matched with the standard data. The diffraction peaks observed at 18.15°, 27.80°, 29.75°, 33.37°, 36.68°, 41.16°, 46.60°, 52.79°, 55.10°, 57.39°, 61.72°, 70.10° and 72.04° are assigned to (2 1 1), (3 2 1), (4 0 0), (4 2 0), (4 2 2), (5 2 1), (5 3 2), (4 4 4), (6 4 0), (6 4 2), (8 0 0), (8 4 0) and (8 4 2) planes, respectively. The average crystallite size of the phosphor is calculated using Debye–Scherrer formula:

$$D = \frac{0.9\lambda}{\beta \cos\theta}, \tag{1}$$

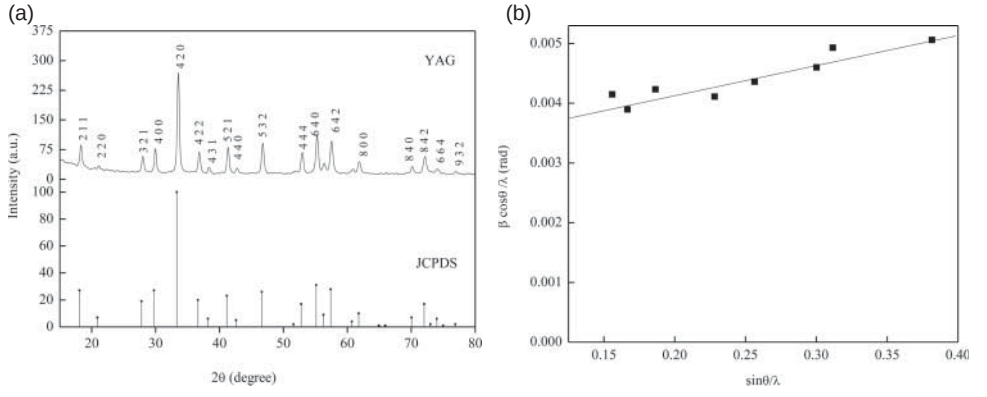

Figure 1. (a). X-ray powder diffraction patterns of $Y_3Al_5O_{12}$. (b) Williamson–Hall plot of 900 °C heat-treated combustion synthesized $Y_3Al_5O_{12}$.

where D is the average crystallite size, λ is the wavelength of X-rays used, β is the full-width at half-maximum (FWHM) of the diffraction peak (in radians) and θ is the diffraction angle. The crystallite sizes are calculated for different peaks and the average crystallite size is estimated to be 20.5 nm. Also, the FWHM of a given diffraction peak may be expressed as a linear combination of the contributions from the lattice strains and the small grain size through the Williamson–Hall relation (*15*) given below

$$\frac{\beta \cos\theta}{\lambda} = \frac{1}{D} + \frac{4\varepsilon \sin\theta}{\lambda}, \tag{2}$$

where ε is the effective strain. A plot of $(\beta \cos\theta)/\lambda$ versus $(\sin\theta)/\lambda$ is shown in Figure 1(b). From the linear fit, the crystallite size is calculated from the Y-intercept and the lattice strain (ε) from the slope of the fit. The crystallite size and the lattice strain are found to be 26.7 nm and 0.126%, respectively. The SEM image of annealed YAG is shown in Figure 2. It can be seen that some agglomeration exist in the powder form and seems to be spongy, volcano in nature which are attributed to the liberation of large quantity of gasses during combustion and formation of necks during annealing (*16*).

TL glow curves of combustion synthesized YAG samples γ-irradiated for doses in the range 1.0–14.0 kGy are given in Figure 3. TL glow curves are recorded at a heating rate of 5 K s^{-1}. Two TL glows: a prominent one with a peak at 410 K resulting from the recombination of F center electron *s* with hole centers and a weak one with a peak at 575 K might be due to the recombination of F^+ center electron with another type of hole centers are observed in all samples (*17*, *18*). The variations of TL glow peak intensity and TL glow peak temperature with γ-dose are shown in Figure 4. It is found that TL intensity of the prominent glow (410 K) peak intensity is observed to increase linearly up to the dose of ∼12.0 kGy and then decreases with a further increase in the γ-dose. And, the glow peak intensity at 575 K is found to increase up to ∼4 kGy, then reaches saturation with a further increase in the γ-dose in the present work (*19*). This indicates that the electron and hole trap centers and hence the recombination events are increased with an increase in γ-doses and hence the TL glow peak intensity increases (*20*). Decrease in TL intensity with further increasing γ-dose may be ascribed to the formation of complex defects or non-radiative centers (*21*). Further, it is observed that the prominent TL glow peak temperature (410 K) is found to be steady with an increase in the γ-dose within the experimental errors.

While studying the crystal structure and luminescence properties of nanocrystalline YAG synthesized by sol–gel method Zhydachevskii and coworkers observed broad TL glows with peaks around 400 and 570 K and a wide emission band with a peak around 800 nm under 1 kGy γ-irradiation (*14*). They attributed the emission due to intrinsic defects of YAG. Vijay Singh et al.

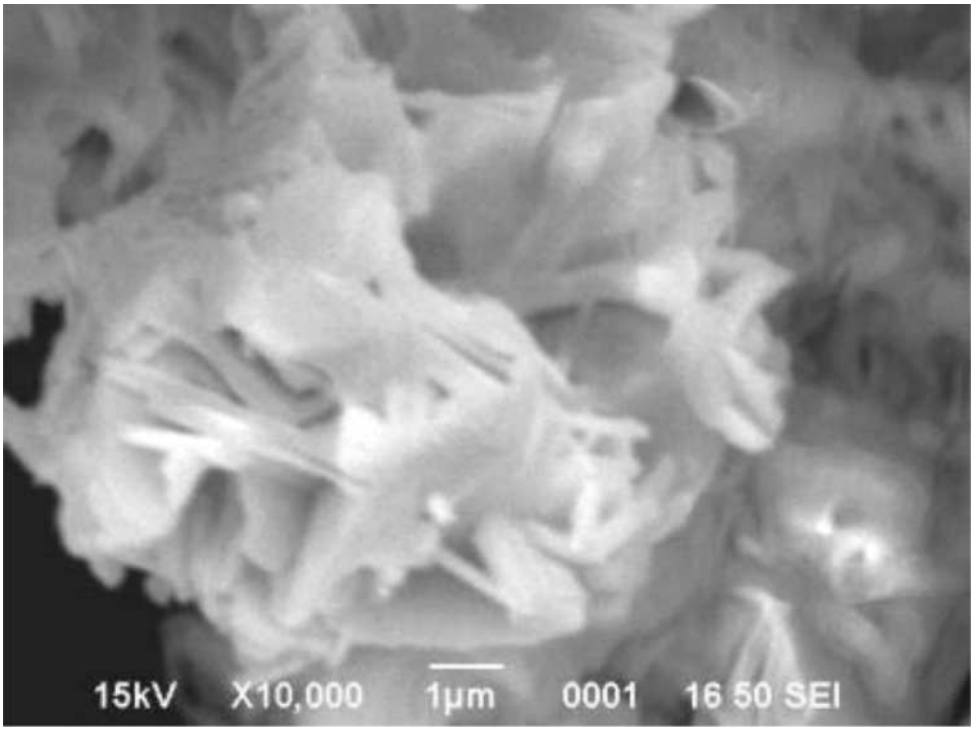

Figure 2. SEM image of 900 °C heat-treated combustion synthesized $Y_3Al_5O_{12}$.

(*17*) reported three TL glows with peaks at 413, 483 and 718 K in glycine–nitrate combustion synthesized 100 Gy γ-irradiated YAG samples. The TL glows with peaks at 413 and 483 K were found to be weak when compared to 718 K TL glow. They attributed TL glows below 673 K to *F*-type centers and above 673 K to F^+-centers using electron spin resonance (ESR) spectroscopy.

Mori (*18*) reported the causes of thermally induced and UV irradiation induced color centers in YAG single crystals using optical absorption spectroscopy, TL and ESR techniques. He observed that primary thermally induced color centers in YAG single crystals were electrons trapped at anion vacancies (F-centers) and the ESR signal showed F^+ and O_h-centers in the crystal. Pujats and Springis (*22*) reported F-type centers in X-irradiated YAG crystals at low temperature. The defects in YAG are mainly oxygen vacancy in the host lattice with one or more trapped electrons which are known as F-type center. In the YAG crystal, the broad photoluminescence band with a peak at 460 nm observed was attributed to presence of the F-center.

The TL of γ-irradiated YAG in the present work exhibits a prominent and broad TL glow with a peak resembling at ~410 K with an overlapping of more than two glows. In order to calculate the accurate values of kinetic parameters one should deconvolute the overlapped TL glows. The deconvolution of the TL glow curves in the present studies performed using computerized glow curve deconvolution based on the Gaussian function using Origin 6.1 software. The deconvoluted TL glow curves are obtained for the best fit of theoretical curve with the experimental one. In the present work, theoretical fit matches with experimental data for four deconvoluted curves. In this method, the area under the curve, the glow peak temperature and the temperature on the lower and upper sides corresponding to half the peak intensity (T_m, T_1 and T_2), and glow peak intensity parameters are obtained (*23*–*25*).

The TL curve of 4.0 kGy γ-irradiated sample shown in Figure 3 is deconvoluted and results are shown in Figure 5(a) for a typical case. Based on this, three TL glows were resolved with peaks

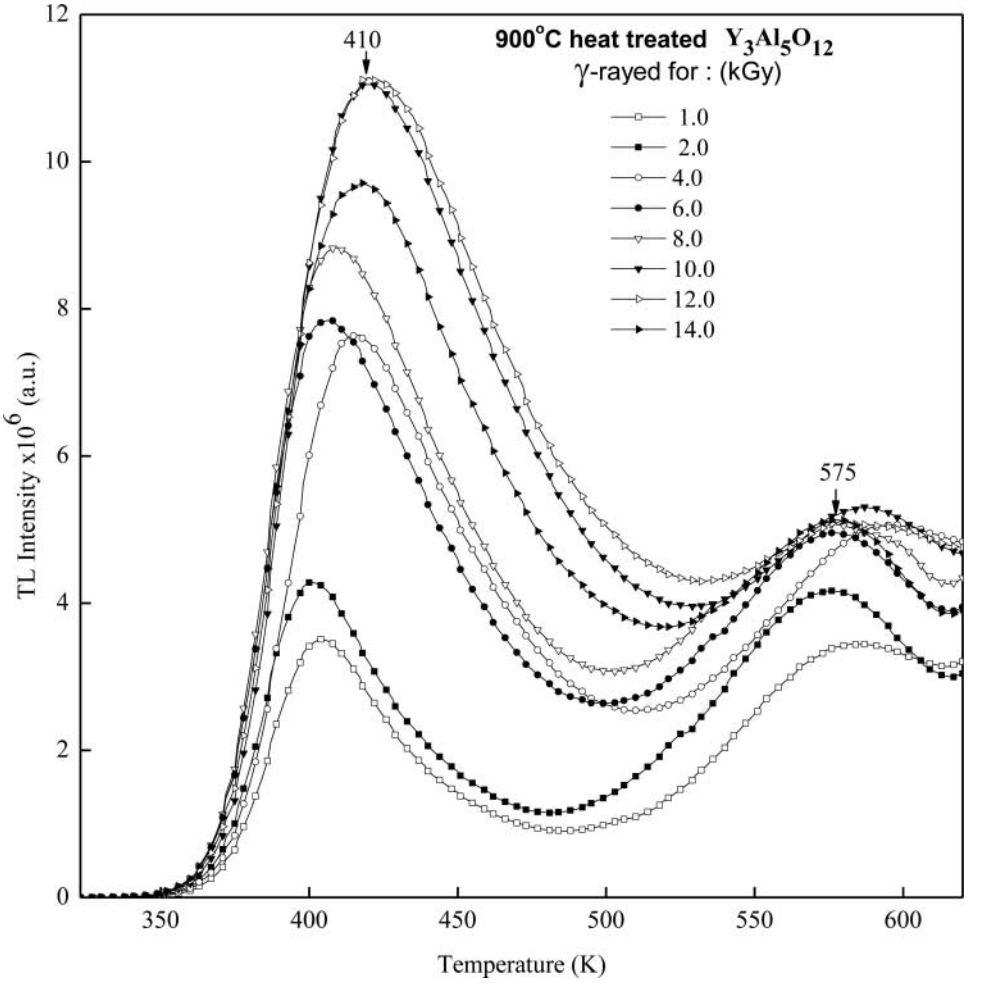

Figure 3. Thermoluminescence glow curves of combustion synthesized γ-irradiated nanocrystalline $Y_3Al_5O_{12}$.

at 407, 437 and 474 K from the prominent experimental TL glow (410 K). And these glow peaks might be due to recombination of different holes and electrons (*17*). The glow peak at 590 K might be due to complex defect center. The variations of deconvoluted TL glow peaks intensity and TL glow peak temperature with γ-dose are shown in Figures 5(b) and 5(c), respectively. It is found that TL intensity of the 407 K glow is found to increase with an increase in the γ-dose up to 12.0 kGy and then decreases with a further increase in the γ-dose. The increase of 407 K glow peak intensity (I_{m1}) is observed to be linear up to the dose of ~10.0 kGy and the glow peaks intensity of second (I_{m2}) and third (I_{m3}) also increases with an increasing γ-dose and the fourth glow peak intensity (I_{m4}) is found to increase up to ~4 kGy, then it saturates with a further increase in the γ-dose. And, the glow peak temperature of the TL glows in the present work are found to be steady with increase in the γ-dose and each of the isolated Gaussian TL glow peak has different FWHM values.

The evaluation of kinetic parameters such as activation energy (E) of the traps involved in TL emission, order of kinetics (b), frequency factor (s) and trap density (n_o) of luminescence centers is one of the important studies in luminescence subject. Here, the energy required to detrap the electron from the trapping center to reach the conduction band (E) and the frequency factor (s)

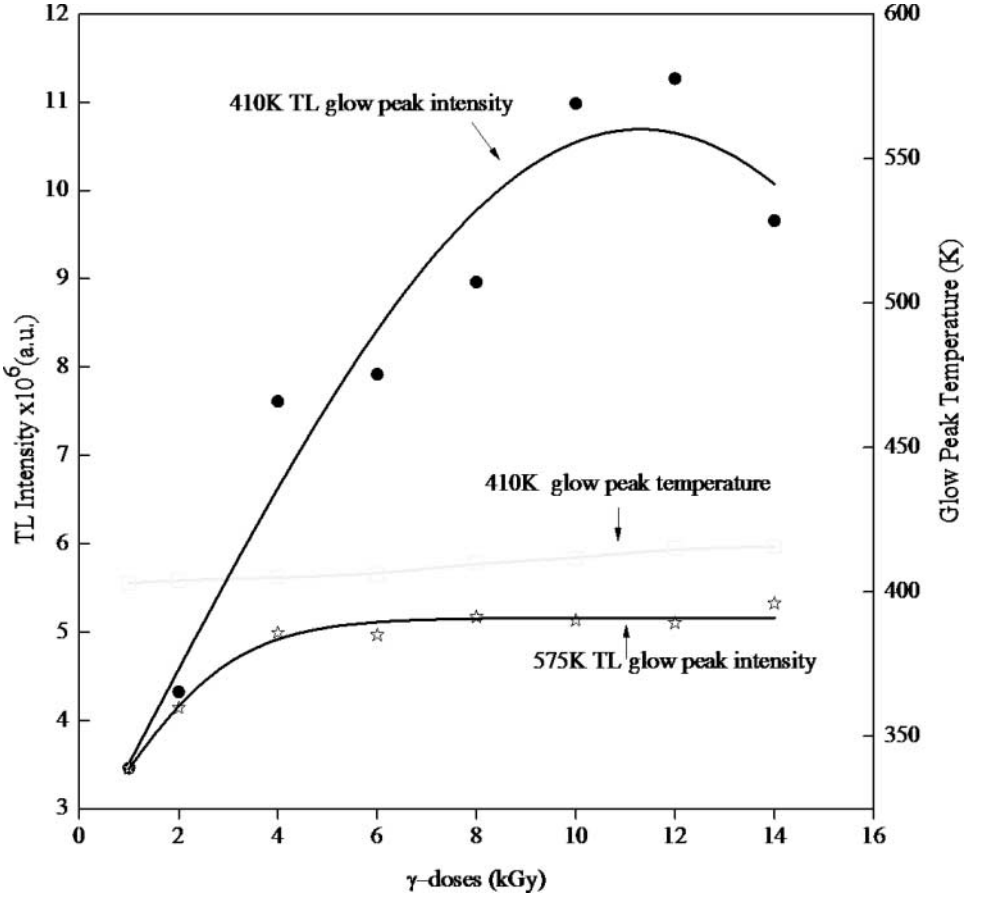

Figure 4. Variation of TL intensity and glow peak temperature with γ-irradiated $Y_3Al_5O_{12}$.

that is the rate of electron ejection. The order of kinetics, b is a measure of the probability that a free electron gets retrapped. The retrapping effect increases with the density of empty traps. The kinetics parameters pertaining to the glow peak are calculated using the glow curve shape method modified by Chen as shown in Figure 5(d) (*26*, *27*) and the values for a typical dose of 4 kGy are given in Table 1. The equations involved in the glow curve shape method are given elsewhere (*28*):

$$\mu_g = \frac{T_2 - T_m}{T_2 - T_1}, \tag{3}$$

where μ_g is the symmetry factor. The temperatures T_m, T_1 and T_2, are, the glow peak temperature and temperature on the lower and upper sides corresponding to half the peak intensity, respectively. The activation energy (E) is calculated using the relation

$$E_\alpha = C_\alpha \frac{kT_m^2}{\alpha} - b_\alpha(2KT_m), \tag{4}$$

where $\alpha = \tau, \delta, \omega$ with $\tau = T_m - T_1$ is the half-width at the low temperature side of the peak; $\delta = T_2 - T_m$ is the half-width towards the fall-off side of the glow peak and $\omega = T_2 - T_1$ is the

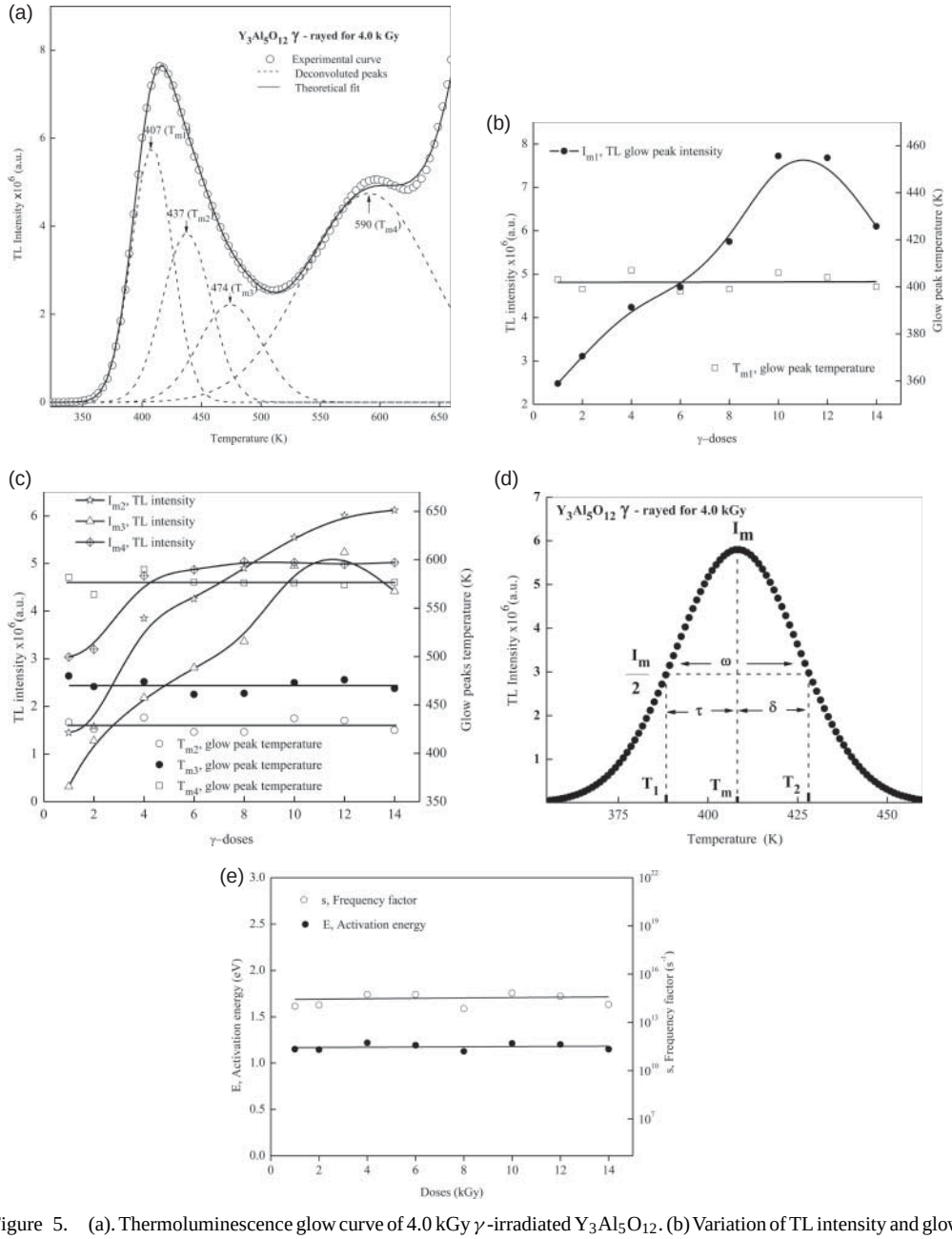

Figure 5. (a). Thermoluminescence glow curve of 4.0 kGy γ-irradiated $Y_3Al_5O_{12}$. (b) Variation of TL intensity and glow peak temperature with γ-irradiated $Y_3Al_5O_{12}$. (c) Variation of TL intensity and glow peak temperature with γ-irradiated $Y_3Al_5O_{12}$. (d) Representative diagram of different parameters used in the glow curve shape method. (e) Variation of activation energy and frequency factor corresponding to T_{m1} as a function of dose.

total half-width and

$$C_\tau = 1.51 + 3.0(\mu_g - 0.42), \quad b_\tau = 1.58 + 4.2(\mu_g - 0.42), \quad C_\delta = 0.976 + 7.3(\mu_g - 0.42),$$
$$b_\delta = 0, \quad C_\omega = 2.52 + 10.2(\mu_g - 0.42), \quad b_\omega = 1.$$

Here, $\mu_g = \delta/\omega$ is the so-called geometrical shape or symmetry factor.

Table 1. Trap parameters of TL glow of 4 kGy γ-irradiated YAG nanocrystalline powder.

TL Peak	T_m (K)	μ_g	Order of kinetics	E (eV)	s (s^{-1})	Trap density n_o (cm^{-3})
T_{m1}	407	0.52	2.0	1.2192	5.43×10^{14}	9.66×10^5
T_{m2}	437	0.51	1.6	1.0151	1.59×10^{11}	1.10×10^7
T_{m3}	474	0.51	1.6	0.8994	8.43×10^8	8.08×10^6
T_{m4}	590	0.50	1.6	0.5996	1.23×10^4	3.60×10^7

The frequency factor is obtained from the relation:

$$\frac{\beta E}{kT_m^2} = s \exp \frac{-E}{KT_m}[1 + (b-1)\Delta_m], \tag{5}$$

where $\Delta_m = 2KT_m/E$, b is the order of kinetics, k is the Boltzmann constant (8.6×10^{-5} eV K^{-1}) and β is the linear heating rate (5 K s^{-1}).

And trap density (n_o) is calculated using the relation (*29*).

$$n_o = \frac{\omega I_m}{\beta\{2.52 + 10.2(\mu_g - 0.42)\}}, \tag{6}$$

where $\omega = T_2 - T_1$, β is the heating rate and μ_g is the symmetry factor.

The activation energy and the frequency factor pertaining to the prominent TL glow in YAG are obtained by the deconvolute method for various dose levels are shown in Figure 5(e). It is found that activation energy and frequency factor is almost steady throughout dose levels. Therefore, the trap depth and the rate of electron ejection from the trap are not affected by dose levels. The activation energy, frequency factor, symmetry factor and trap density pertaining to T_{m1} are estimated to be 1.1734 eV, 3.2334×10^{14} s^{-1}, 0.52 and 8.6023×10^6 cm^{-3}, respectively. The prominent glow peak (T_{m1}) obeys the second-order kinetics, and the other three glow peaks as analyzed above are found to obey the general order kinetics.

The effective atomic number ($Z_{effective}$) is a fundamental property of the TL materials and it is related with radiation interaction processes and the latter has direct applications in characterization of wide range of radiological dosimetry and surrogate materials and biological tissues and the calculation of particle interactions. For practical applications, such as high sensitivity of TL material must have high $Z_{effective}$ atomic numbers. For ionizing radiation, the material factor governing the energy dependence is the effective atomic number (Z_{eff}), which indicates the amount of energy absorbed by the material by a given radiation. The higher the value of Z_{eff} and the lower the energy of incident photons, the larger is the TL response to a given dose due to the dominant component of the photoelectric effect in the mass energy absorption coefficient. The effective atomic number has been calculated using a simple power law of the form:

$$Z_{eff} = \sqrt[m]{\sum_i a_i Z_i^m}, \tag{7}$$

where a_i is the fractional electron content of element 'i' with the atomic number Z_i. The value of m will typically be in the range 3–4, with 3.5 being a reasonable value (*30*). The Z_{eff} of $Y_3Al_5O_{12}$ compound has been calculated to be 30.58. Therefore, YAG has a high effective number hence is used in radiological dosimetry applications (*12*).

The heating rates have a pronounced effects on the trapping parameters of TL materials provided the TL material responses effectively. Therefore, the heating rate is one of the most important experimental parameters which strongly affect the TL glow intensity, glow curve temperature and FWHM (*31*). Figure 6(a) shows the TL glow curves of YAG recorded at three typical heating rates.

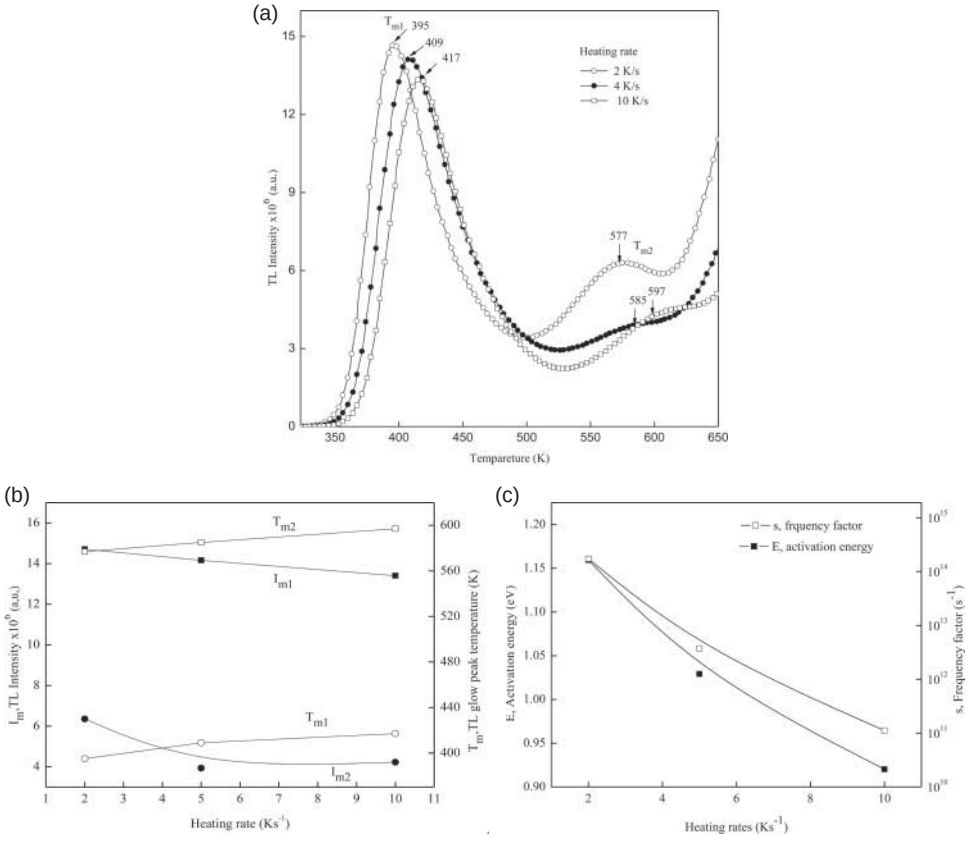

Figure 6. (a). Effect of heating rates on TL glow curve for samples exposed to 5 kGy γ-dose. (b) Variation of TL intensity and glow peaks temperature of the defect centers corresponding to T_{m1} and T_{m2} as a function of heating rates. (c) Variation of activation energy and frequency factor of the defect center with T_{m1} as a function of heating rates.

The prominent glow peak temperature (T_{m1}) observed at ~395 K is found to be shifted towards higher temperature side while decreasing in intensity (I_{m1}) and FWHM increases with an increase in the heating rate as shown in Figure 6(b). This may be attributed to thermal quenching of TL due to an increase in the heating rate (*32*). Figure 6(c) shows variation of activation energy and frequency factor as a function of heating rate. It is found that activation energy and frequency factor decrease with increase in heating rates. Therefore, trap depth and the rate of electron ejection seems to be dependent on heating rates.

4. Conclusions

Nanocrystalline YAG phosphor is synthesized by combustion technique using urea as the fuel. XRD pattern revealed the cubic phase and the average crystallite sizes are found to be ~20.5 nm. The SEM picture of YAG indicated the spongy and volcano-type morphology. Two well-resolved TL glows – a prominent one with a peak at ~410 K and another one with a peak at 575 K are observed in all γ-irradiated samples. It is found that the prominent TL glow peak (410 K) intensity increases linearly up to about 12 kGy γ-dose. This glow peak may be considered for radiation dosimetric applications. The TL glow curves are analyzed by Chen's peak shape method and the TL parameters are estimated. The experimental TL glow curve is composed of overlapping TL

peaks around 407, 437, 474 and 590 K. And the glow peak intensity of 407 K glow is found to linearly increased up to 10.0 kGy γ-dose. The prominent TL glow obeys the second-order kinetics since the retrapping of electron is high.

Acknowledgements

The authors express their sincere thanks to Dr. D.K. Avasthi, Materials Science Division & Dr. S.P. Lochab, Health Physics Division, Inter University Accelerator Centre, New Delhi, India for their constant encouragement and help during the experiment. Also, one of the authors (NJS) is grateful to Inter University Accelerator Centre, New Delhi, India for providing fellowship under UFR (No. 48303) scheme.

References

(1) French, J.D.; Zhao, J.; Harmer, M.P.; Chan, H.M.; Miller, G.A. *J. Am. Ceram. Soc*. **1994**, *77*, 2857–2865.
(2) Xu, Y.N.; Ching, W.Y. *Phys. Rev. B*. **1999**, *59*, 10530–10535.
(3) Shannon, R.D.; Subramanian, M.A.; Allik, T.H.; Kimura, H.; Kokta, M.R. *J. Appl. Phys*. **1990**, *67*, 3798–3802.
(4) Hofmeiser, A.M.; Campbell, K.R. *J. Appl. Phys*. **1992**, *72*, 638–646.
(5) Stoddart, P.R.; Ngoepe, P.E.; Mjwara, P.M.; Comins, J.D.; Saunders, G.A. *J. Appl. Phys*. **1993**, *73*, 7298–7301.
(6) Alton, W.J.; Barow, A.J. *J. Appl. Phys*. **1967**, *32*, 3023–3024.
(7) De la Rosa, E.; Diaz Torres, L.A.; Salas, P.; Arredondo, A.; Montoya, J.A.; Angeles, C.; Rodriguez, R.A. *Opt. Mater.* **2005**, *27*, 1793–1799.
(8) Ashurov, Kh.M.; Rakov, A.F.; Erzin, R.A. *Solid State Commun*. **2001**, *120*, 491–494.
(9) Rodriguez, R.A.; De la Rosa, E.; Daiz-Torres, L.A.; Salas, P.; Melendrez, R.; Barboza-Flores, M. *Opt. Mater*. **2004**, *27*, 293–299.
(10) Kingsley, J.J.; Suresh, K.; Patil, K.C. *J. Solid State Chem*. **1990**, *87*, 435–442.
(11) Mckeever, S.W.S. *Thermoluminescence of Solids*; Cambridge University Press: Cambridge, 1985.
(12) Furetta, C. *Handbook of Thermoluminescence*; World Scientific Publishing: Singapore, 1937.
(13) Yoshimura, E.M.; Yukhihara, E.G. *Nucl. Instrum. Methods B* **2006**, *250*, 337–341.
(14) Zhydachevskii, Y.; Syvorotka, I.I.; Vasylechko, L.; Sugak, D.; Borshchyshyn, I.D.; Luchechko, A.P.; Vakhula, Y.I.; Ubizskii, S.B.; Vakiv, M.M.; Suchocki, A. *Opt. Mater*. **2012**, *34*, 1984–1989.
(15) Khorsand Zak, A.; Abd, W.H.; Majid Abrishami, M.E.; Yousefi, R. *Solid State Sci*. **2011**, *13*, 251–256.
(16) Hassanzadeh Tabrizi, S.A. *Trans. Nonferrous Met. Soc. China* **2011**, *21*, 2443–2447.
(17) Singh, V.; Rai, V.K.; Watanabe, S.; Gundu Rao, T.K.; Ledoux Rak, I.; Kwak H.-Y. Kwak. *Appl. Phys A.: Mater. Sci. Process.* **2010**, *100*, 1123–1130.
(18) Mori, K. *Phys. Status Solidi A* **1977**, *42*, 375–384.
(19) Lawless, J.L.; Chen, R.; Lo, D.; Pagonis, V. *J. Phys.: Condens. Matter* **2005**, *17*, 37–753.
(20) Prashantha, S.C.; Lakshminarasappa, B.N.; Singh, F. *J. Lumin*. **2012**, *132*, 3093–3097.
(21) Lachab, S.P.; Sahare, P.D.; Chauhan, R.S.; Salah, N.; Ranjan, R.; Pandey, A. *J. Phys. D: Appl. Phys.* **2007**, *40*, 1343–1350.
(22) Pujats, A.; Springis, M. *Radiat. Eff. Def. Solids* **2001**, *155*, 65–69.
(23) Furetta, C.; Kittis, G.; Kuo, C.H. *Nucl. Instrum. Methods B* **2000**, *160*, 65–72.
(24) Vij, A.; Lochab, S.P.; Singh, S.; Kumar, R.; Singh, N. *J. Alloys Compd*. **2009**, *486*, 554–558.
(25) Salah, N.; Habib, S.S.; Khan, Z.H.; Al-Hamedi, S.; Lochab, S.P. *J. Lumin.* **2009**, *129*, 192–196.
(26) Chen, R.; Krish, Y. *Analysis of Thermally Stimulated Processes*; Pergamon Press: New York, 1981; pp 162–173.
(27) Furetta, C. *Handbook of Thermoluminescence*; World Scientific: Singapore, 2003; pp 260–276.
(28) Nagabhushana, K.R.; Lakshminarasappa, B.N.; Singh, F. *Radiat. Meas*. **2008**, *43*, S651–655.
(29) Suriyamurthy, N.; Panigrahi, B.S. *J. Lumin.* **2008**, *128*, 1809–1814.
(30) Bos, A.J.J. *Nucl. Instrum. Methods B*. **2001**, *184*, 3–28.
(31) Necmeddin yazici, A.; Yakup haci ibrahimoglu, M.; Bedir, M. *Turk. J. Phys*. **2000**, *24*, 623–649.
(32) Sharm, G.; Chawla, P.; Lochab, S.P.; Singh, N. *Chalcogenide Lett*. **2009**, *6*, 445–453.